2010 Southern California Earthquake Center Annual Report
Integrated studies of material damage, nonlinear ground motion and high-frequency radiation bursts

Zhigang Peng (PI)
School of Earth and Atmospheric Sciences
Georgia Institute of Technology, Atlanta, GA, 30338
March 18, 2011

Summary

A systematic analysis of nonlinear site response and damage related radiation is very important for better understanding nonlinear strong ground motion and temporal changes of material properties in the shallow crust. The information is critical for accurate prediction of strong shakings during large earthquakes. Our past year's effort mainly focused on the following two directions: (1) Separating genuine bursts of high frequency radiation from apparent bursts produced by analysis artifacts (Peng et al., 2011); (2) Identifying the threshold of peak ground acceleration (PGAs) that separates effects of nonlinear response with and without material damage (Wu et al., 2010a, 2010b).

1. Separating genuine bursts of high frequency radiation from apparent bursts produced by analysis artifacts (Peng et al., 2011)

Recently studies have shown that shallow high-frequency earthquakes and deep low-frequency tremor can be triggered by surface waves of large distant earthquakes [Peng and Gomberg, 2010; and reference therein]. In addition, several groups have documented high-frequency bursts in the extremely shallow crust during the strong ground motions of the 1999 Mw7.6 Chi-Chi (Chen et al. 2006; Fischer et al. 2008a) and 2004 Mw6.0 Parkfield earthquakes (Fischer et al. 2008b; Sleep and Ma 2008). It is still not clear whether those two types of triggered signals are related or not. An effective way to demonstrate and identify triggered signals is spectrogram display, where the triggered event is characterized with elevated high-frequency spikes during large-amplitude and long-period surface waves.

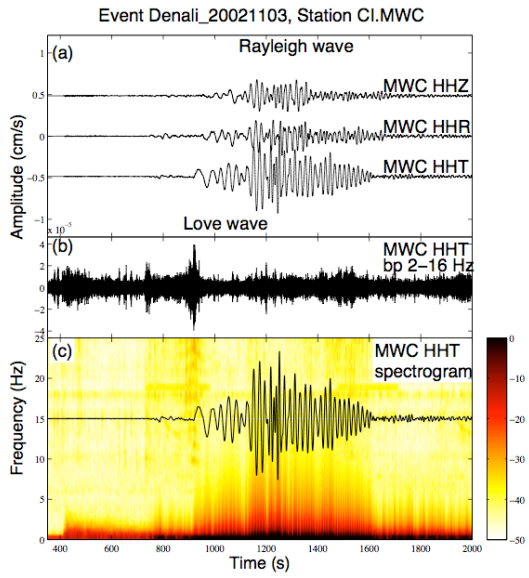

Figure 1. (a) Instrument-correlated 3-component seismograms generated by the 2002 Mw7.8 Denali Fault earthquake and recorded at the broadband station CI.MWC in Southern California. (b) 2-16 Hz band-pass-filtered transverse-component seismogram showing locally generated high-frequency signals. (c) The spectrogram of the transverse-component seismogram at station CI.MWC shaded by the amplitude in db below the maximum.

Figure 1 shows an example of the original 3-component broadband seismograms (HH channels), 2-16 Hz band-pass-filtered transverse component, and the corresponding spectrogram recorded by the station MWC near the Mount Wilson Observatory on the SGM. This station recorded weak tremor triggered by the 2002 Denali Fault earthquake (Fabian *et al.*, 2009). A general pattern in the spectrogram from this and other stations equipped with broadband seismometer/digitizer systems is bursts of high-frequency energy during the large-amplitude surface waves. A zoom-in examination reveals that the high-frequency energy is mostly

centered on the zero crossing in the broadband seismograms. In comparison, the spectrogram from the short-period recordings (EH channel) at the same station does not show elevated high-frequency energy during the long-period surface waves. Finally, such high-frequency energy is not shown in the 2-16 Hz band-pass-filtered seismograms. Hence, we suspect that such high-frequency signals are likely caused by the signal analysis procedures.

To further support the above hypothesis, we generate a synthetic seismogram from a pure sine function with 20-s period that mimics the typical 20-s surface waves with the same sampling rate (100/s). Elevated high-frequency energy in the spectrogram is centered on the zero crossing of sine function (Figure 2), similar to the observations from the real data (e.g., Figure 1). This demonstrates that the high-frequency energy in the spectrogram must originate from the procedure to compute spectrograms with multiple short-time windows. Through additional synthetic example, we find that when the length of the window used to computed the FFT and the spectrogram is smaller than the wavelength of the seismic waves (i.e., during large-amplitude long-period surface waves), the windowing effect is amplified.

After we identify the cause of such high-frequency artifact, we propose the following three approaches (Figure 3) to remove or reduce such high-frequency artifacts: 1. Applying a high-pass filter to reduce long period noises that cannot be resolved by the short-time windows; 2. Using narrow band-pass filtering (instead of short time windows) to compute the spectrogram; and 3. Computing the spectrum using the Burg method. All these approaches resulted in clean spectrogram that match the band-pass-filtered seismogram and the spectrogram from collocated

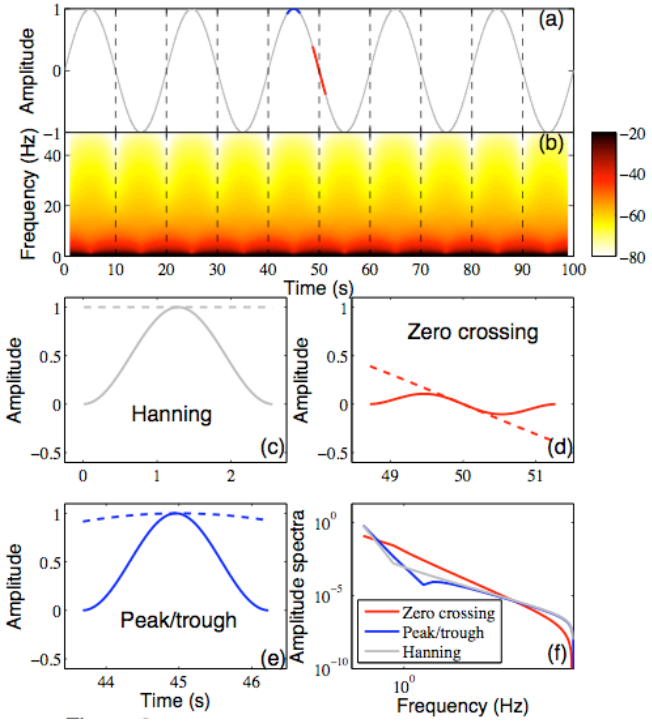

Figure 2. (a) A sine function with a period of 20 s. (b) The spectrogram. (c) The Hanning window (solid) and data with amplitude = 1 (dashed). (d) The truncated data around zero crossing (dashed) and after applying the Hanning window (solid). (e) The truncated data around the peak/trough (dashed) and after applying the Hanning window (solid). (f) The Fourier spectra of the Hanning window (light gray), the windowed zero crossing (gray), and windowed peak/trough (black).

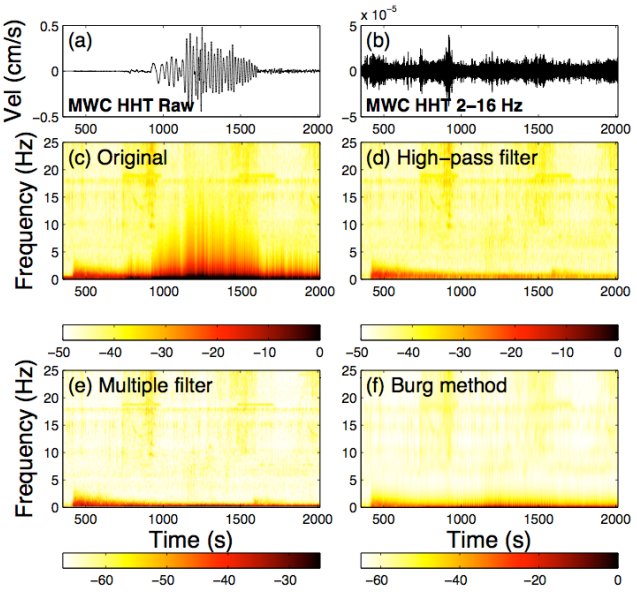

Figure 3. (a) Three sine functions with the same phase (30°) and slightly different frequencies. (b) The Fourier spectra of the sine functions shown in (a). (c) The Burg spectra of the sine functions shown in (c). We use the *Matlab*^{R} command *pburg*(*x*,*p*,*nfft*,*fs*) with *p* = 30 and *nfft* = 4096. See texts for detailed description of each parameter. (d) Three sine functions with the same frequency (0.5 Hz) and different phases. (e) The Fourier spectra of the sine functions shown in (c). (f) The Burg spectra of the sine functions shown in (d).

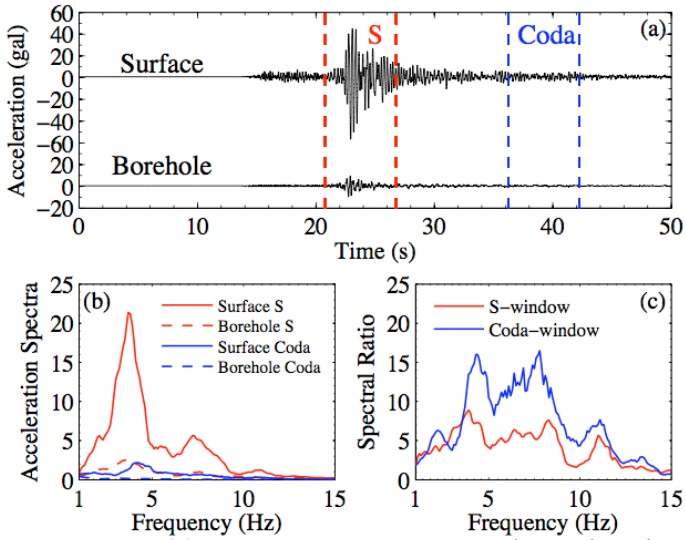

Figure 4. (a) East-component ground accelerations recorded at the station NIGH06 generated by an M5.3 earthquake on Oct 25, 2004. Surface recording is shown at the top and borehole recording is shown at the bottom. The red and blue dashed lines indicate the direct *S* and coda window that are used to compute the acceleration spectra in (b) and spectral ratios in (c).

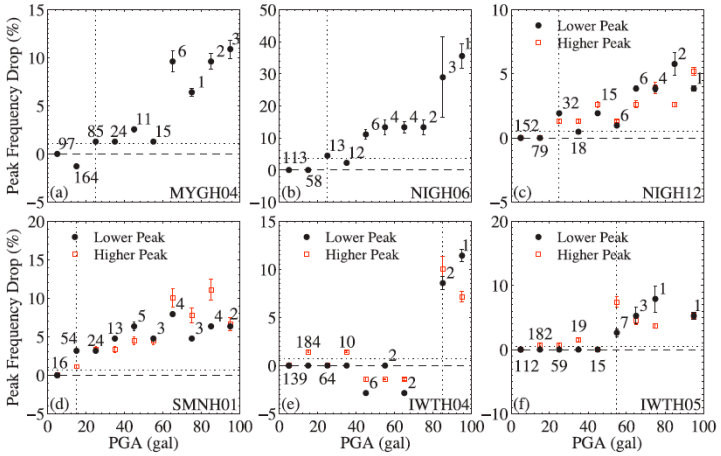

Figure 5. Percentage drop of the peak frequency plotted against the PGA for the 6 stations (a-f). The black solid circles and red open squares mark the values measured from the 6-s windows immediately after the direct *S*-wave arrivals for the lower and higher resonance peaks, respectively. The vertical solid bar centered at each data point shows the standard deviation, with the number of stacked events by its side. The horizontal dashed line indicates the zero level. The horizontal dotted line marks 10% of the value measured at 90-100 gal. The vertical dotted line marks the inferred PGA threshold of nonlinearity. The station name is marked at the bottom-right corner of each panel.

short-period station well, suggesting that the aforementioned high-frequency artifact has been largely reduced. Because the spectrogram plot is useful to identify and demonstrate remotely triggered seismic activity (e.g., West *et al.*, 2005; Hill and Prejean, 2007; Peng and Chao, 2008; Peng *et al.*, 2008), it is important to identify such potential artifact, and use the proper approaches mentioned above to compute the correct spectrogram so that no false interpretation is made.

2. Identifying the PGA threshold that separates effects of nonlinear response with and without material damage (Wu et al., 2010a, 2010b)

In the second work, we conducted a systematic search of the PGA threshold that separates effects of nonlinear response with and without material damage in Japan (Wu et al., 2010a) and California (Wu et al., 2010b). We first analyze nonlinear effects and temporal changes of site response associated with medium-size earthquakes recorded by the Japanese Strong Motion Network KIK-Net. We applied a sliding-window spectral ratio technique to surface and borehole strong motion records at 6 sites, and stack results associated with different earthquakes that produce similar peak ground acceleration (PGA). Figure 4 shows an example of the original acceleration records at NIGH06 generated by an M5.3 event on 10/25/2004 and the 6-s windows used to compute the spectral ratios for the direct *S* and coda waves. By comparing the spectral ratios, we identify a clear shift of resonant frequency around 4 Hz to lower values and a drop in peak amplitude for the direct *S* waves (Figure 4c). Both of these features are hallmarks of nonlinear site effects.

After processing all the data, we group the events in different PGA ranges (0-100 gal with an increment of 10 gal) and stack the spectral ratio traces from 12 s before to

60 s after the *S*-wave arrival time within each group. As before, we tested stacking the trace using different PGA ranges, and the obtained results are similar. Next, we identify the peak spectral ratio and peak frequency for the stacked trace in each PGA range. Figure 5 shows that in some cases we observe a weak coseismic drop in the peak frequency when the PGA is as small as ~20-30 gal, and near instantaneous recovery after the passage of the direct *S* waves. The percentage of drop in the peak frequency starts to increase with increasing PGA values. We also observe a coseismic drop in the peak spectral ratio for 2 sites. When the PGA is larger than ~60 gal to more than 100 gal, we observe considerably stronger drops of the peak frequencies followed by logarithmic recovery with time. The observed weak reductions of peak frequencies with near instantaneous recovery likely reflect nonlinear response with essentially fixed level of damage, while the larger drops followed by logarithmic recovery reflect the generation (and then recovery) of additional rock damage. The results indicate clearly that nonlinear site response may occur during medium-size earthquakes, and that the PGA threshold for *in situ* nonlinear behavior is lower than the previously thought value of ~100-200 gal.

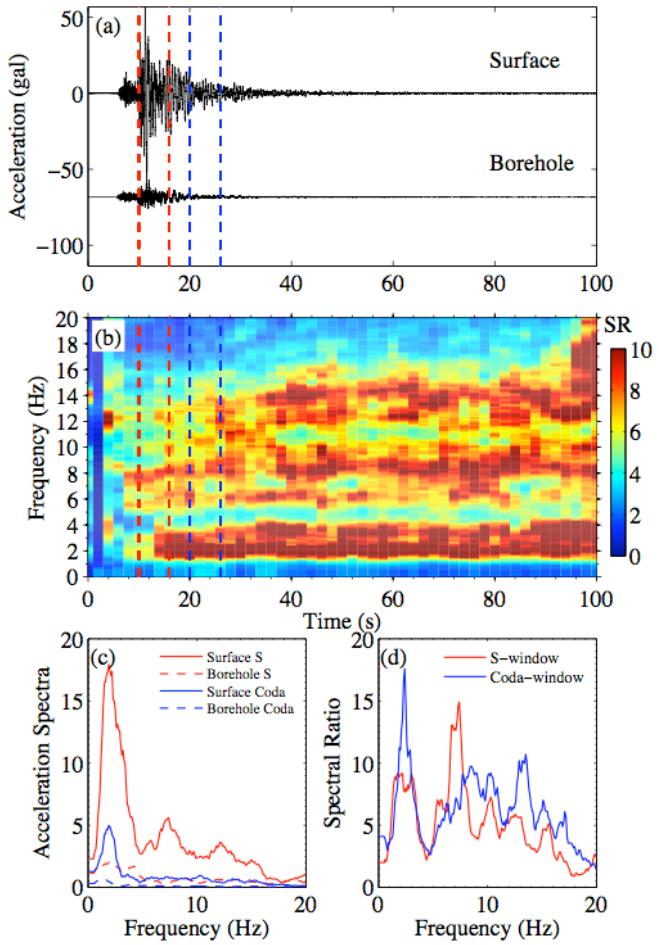

Figure 6. (a) NS-component ground accelerations recorded at the station GVDA generated by the M5.4 Collins Valley earthquake on July 07, 2010. Surface recording is shown at the top and borehole recording is shown at the bottom. The red and blue dashed lines indicate the direct S and coda window that are used to compute the acceleration spectra in (c) and spectral ratios in (d). (b) Sliding-window spectral ratios of the surface and borehole recordings shown in (a). X-axis is the time from 10 s bwfore to 90 s after the S-wave arrival, and y-axis is the frequency. The horizontal white dashed line marks the reference value of the resonance frequency.

The 2010/04/04 Mw7.2 El Mayor-Cucapah Earthquake in northern Baja California has triggered a widespread increase of moderate-size earthquakes in southern California (Peng et al., 2010; Haukkson et al., 2010) that are well recorded by many SCEC borehole instruments. We are currently applying the sliding window spectral ratio technique to these newly available data. Figure 6 shows an example of possible peak spectral reduction recorded at the Garner Valley Digital Array (GVDA) during the S wave of the 07/07/2010 Mw5.4 Collins Valley earthquake on Coyote segment of the San Jacinto Fault. Our next step is to systematically analyze all recent moderate events recorded by the GVDA and other downhole array in southern California to better define the nonlinear threshold in this region.

Student Support and Involvement. This project provided half-support for the GT graduate student Chunquan Wu, who has become an export in studying nonlinear site response in California, Japan and Turkey. This work will be part of his Ph.D. thesis on understanding "dynamically induced temporal changes and seismic activity".

References (with publications/meeting abstracts supported by the grant marked in bold)

Chen, Y., C. G. Sammis, and T.-L. Teng (2006), A high frequency view of the 1999 Chi-Chi, Taiwan, Source Rupture and Fault Mechanics, *Bull. Seismol. Soc. Am.,* **96,** 807–820.

Fabian, A., L. Ojha, Z. Peng, and K. Chao (2009), Systematic search of remotely triggered tremor in Northern and Southern California, Eos Trans. AGU, 90(54), Fall Meet. Suppl., Abstract T13D-1916.

Fischer, A. D., C. G. Sammis, Y. Chen, and T. Teng (2008a). Dynamic Triggering by Strong-Motion P and S Waves: Evidence from the 1999 Chi-Chi, Taiwan, Earthquake, *Bull. Seism. Soc. Am.* 98, no. 2, 580.

Fischer, A. D., Z. Peng, and C. G. Sammis (2008b), Dynamic triggering of high-frequency bursts by strong motions during the 2004 Parkfield earthquake sequence, *Geophys. Res. Lett.*, 35, L12305, doi:10.1029/2008GL033905.

Hauksson, E., J. Stock, K. Hutton, W. Yang, A. Vidal-Villegas, and H. Kanamori (2010), The 2010 Mw 7.2 El Mayor-Cucapah earthquake sequence, Baja California, Mexico and southernmost California, USA: active seismotectonics along the Mexican Pacific margin, Pure Appl. Geophys., DOI 10.1007/s00024-00010-00209-00027.

Hill, D. P., and S. G. Prejean (2007). Dynamic triggering, in Treatise on Geophysics, 257–292, ed. Schubert, G., Vol. 4: Earthquake Seismology, ed. Kanamori, H., Elsevier, Amsterdam.

Peng, Z., and K. Chao (2008), Non-volcanic tremor beneath the Central Range in Taiwan triggered by the 2001 Mw7.8 Kunlun earthquake, Geophys. J. Int. (Fast track), doi: 10.1111/j.1365-246X.2008.03886.x.

Peng, Z. and J. Gomberg (2010), An integrated perspective of the continuum between earthquakes and slow-slip phenomena, *Nature Geosci.*, 3, 599–607, doi:10.1038/ngeo940.

Peng, Z., J. E. Vidale, K. C. Creager, J. L. Rubinstein, J. Gomberg, and P. Bodin (2008), Strong tremor near Parkfield, CA excited by the 2002 Denali Fault earthquake, Geophys. Res. Lett., 35, L23305, doi:10.1029/2008GL036080.

Peng, Z., X. Meng, and A. Doran (2010), Understanding physical mechanisms of earthquake triggering in southern California following the 2010 Mw7.2 Northern Baja California earthquake, 2010 SCEC Annual Meeting.

Peng, Z., L. T. Long, and P. Zhao (2011), The relevance of high-frequency analysis artifacts to remote triggering, *Bull. Seismol. Soc. Am.*, submitted.

Sleep, N. H. and S. Ma (2008), Production of brief extreme ground acceleration pulses by nonlinear mechanisms in the shallow subsurface, G^3 **9,** no. 3, Q03008.

West, M., J. J. Sanchez, and S. R. McNutt (2005). Periodically triggered seismicity at Mount Wrangell, Alaska, after the Sumatra earthquake. *Science* **308**, 1144–1146; doi:10.1126/science.1112462.

Wu, C., Z. Peng, and Y. Ben-Zion (2010a), Refined thresholds for nonlinear ground motion and temporal changes of site response associated with medium size earthquakes, *Geophys. J. Int.*, 183, 1567-1576, doi: 10.1111/j.1365-246X.2010.04704.x.

Wu, C., Z. Peng, and Y. Ben-Zion (2010b), Nonlinear ground motion and temporal changes of site response associated with medium-size earthquakes in Japan and California, *2010 SCEC Annual Meeting*.